Slots and Complementary Split Ring Resonators Loaded Miniaturized Microstrip Antenna (S-CSRR-MHMSA) with Reduced Cross Polarization

Uday A. Patil^{1,}* and Anandrao B. Kakade^2

Abstract—Cross polarization (X-pol) effect is the undesired radiation of an antenna which wastes bandwidth(BW) and power of the communication system. Especially in the miniaturized microstrip antenna (MSA) the X-pol level is more. The observed X-pol level of the classical MSA at the direction of maximum radiation ($\phi = 0°$) is -49.72 dB, whereas X-pol level of miniaturized H shaped MSA (MHMSA) is -39.96 dB. This paper presents miniaturized complementary split ring resonators loaded H shaped microstrip antenna (CSRR-MHMSA) and slots and CSRRs loaded MHMSA (S-CSRR-MHMSA) with reduced X-pol level. An array of CSRRs and slots are placed at the ground of the proposed antenna. Due to slots, the antenna is miniaturized and the polarizability of the electric field along the desired direction is increased by CSRRs. The CP-XP (Co-pol X-pol) isolation of CSRR-MHMSA and S-CSRR-MHMSA at $\phi = 0°$ are measured. The measured E plane CP-XP isolation for CSRR-MHMSA and S-CSRR-MHMSA is 29.00 dB and 26.73 dB, respectively. The measured CP-XP H plane isolation for CSRR-MHMSA and S-CSRR-MHMSA is 27.00 dB and 24.5 dB, respectively. While maintaining bandwidth (BW), gain G and radiation efficiency η are improved.

1. INTRODUCTION

Wireless communication system requires compact and handy devices for power saving. This gives rise to the use of miniaturized microstrip patch antenna. It is a popular choice due to its ease of design and conformability. However, it suffers from low gain, low bandwidth (BW), poor efficiency, and a significant level of X-pol. The coaxial feed and microstrip line feed microstrip patch antennas are inherently asymmetrical in structure, so they operate in multiple modes. Antennas operating in multimode suffer from the effect of cross-polarization. In wireless communication system especially in mobile handset low gain and narrow BW are acceptable. However, X-pol should be below the minimum acceptable level for power saving.

There are three definitions of cross-polarization (X-pol) in the literature [1, 2]. They are:

(i) In a Cartesian coordinate system, one unit vector is taken as the Co-pol direction and one unit vector as the X-pol direction.
(ii) In a spherical coordinate system, one unit vector is taken as the Co-pol direction, and one unit vector is in the X-pol direction. Both orthogonal unit vectors are tangent to the spherical surface.
(iii) Co-pol and X-pol define what is measured when patterns are taken in the usual way.

According to IEEE standards, X-pol is defined as "The polarization orthogonal to the Co-polarization". However, there is no unanimously accepted definition of X-pol and Co-pol. One of the definitions can

* Corresponding author: Uday A. Patil (uap_tech@unishivaji.ac.in).
^{1} Department of Technology, Shivaji University, Kolhapur, Maharashtra, India. ^{2} Rajarambapu Institute of Technology, Sakharale, India.

be used to measure the X-pol and Co-pol of an antenna. For the proposed work, a second definition of Co-pol and X-pol has been adopted for antenna radiation pattern measurement.

A number of feeding methods for minimizing cross-polarization have been proposed in the literature. An aperture coupled feed microstrip patch antenna reduces the cross-polarization effect [3, 4]. However, it has a narrow bandwidth. The structure of this feeding technique is complex and generally cannot be used in miniaturized devices. The corner feed technique for microstrip array is useful for reduction of X-pol level [5]. Using this technique -35 dB X-pol level is achieved. Chin et al. [6] have proposed a broad band antenna with low X-pol. The folded plate pair as a differential feeding scheme is applied to the patch antenna for reduction of X-pol level. A meander line ring cavity structure is introduced by Chen et al. [7] for the reduction of X-pol from -14.2 dB to -26.1 dB. Defected ground structure (DGS) is another method for X-pol reduction. Kumar et al. [8] have achieved CP-XP isolation better than 30 dB.

In addition to the above methods, a metamaterial inspired structure can also be used for the reduction of X-pol level. Split ring resonator is one of the versatile structures that can be used to get desired Co-pol and to reduce X-pol levels [9]. Manikandan and Jawahar proposed an array of microstrip antennas with a pure axial ratio [10]. Axial ratio purity is obtained by reducing X-pol, which is achieved by placing split ring resonators between adjacent microstrip antennas. In the proposed work, metamaterial inspired complementary split ring resonators and an array of slots are used to reduce the X-pol of the miniaturized microstrip patch antenna. In Section-2, a miniaturized H shaped microstrip patch antenna (MHMSA) is discussed. In Section-3 and Section-4, the design of CSRR-MHMSA and S-CSRR-MHMSA is discussed. In Section-5 and Section-6, results and conclusion are discussed respectively.

2. DESIGN OF MHMSA

Initially, a microstrip line fed MSA has been designed at a frequency of 2.4 GHz using the transmission line model. The top view of the MSA is shown in Fig. 1(a). The substrate material selected for MSA design is fiber glass FR4 with dielectric constant $\varepsilon_r = 4.4$, loss tangent $\tan\delta = 0.001$, and substrate height $h = 1.6$ mm. The problem of impedance mismatch is minimized using a quarter wave transformer
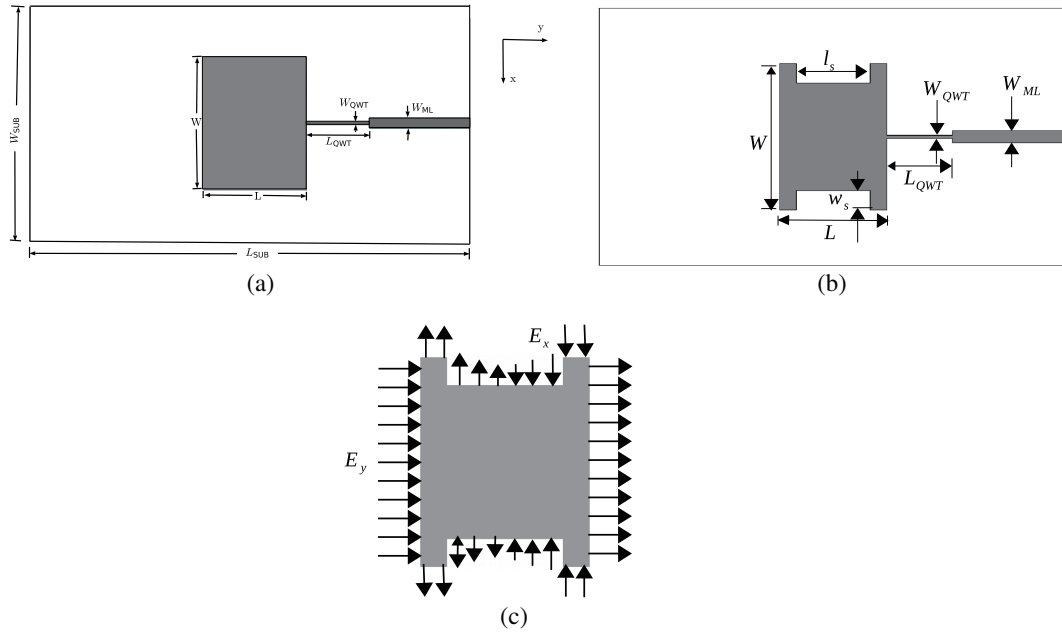

Figure 1. Antenna top view. (a) MSA. (b) MHMSA, CSRR-MHMSA, S-CSRR-MHMSA. (c) Fringing electrical field distribution on MHMSA patch.

(QWT). Dimensions of the MSA are $W_{sub} = 66\,\text{mm}$, $L_{sub} = 127\,\text{mm}$, $L = 29.07\,\text{mm}$, $W = 37.57\,\text{mm}$, $W_{ML} = 3\,\text{mm}$, $L_{QWT} = 17.749\,\text{mm}$, and $W_{QWT} = 0.723\,\text{mm}$. Then the slot-loading MSA technique is used to reduce the size by increasing the path length of the surface current. The path length of the surface current has been increased by cutting the rectangular slot equally at both non-radiating edges, as shown in Fig. 1(b). Dimensions of the rectangular slot are $l_s = 20\,\text{mm}$ and $w_s = 5\,\text{mm}$. The shape of the miniaturized MSA is 'H', so it is called a miniaturized H-shaped MSA (MHMSA). The resonance frequency of the MHMSA for given dimensions is calculated using Eq. (1).

$$f = \frac{c}{2(L_e + 2w_s)} \tag{1}$$

where w_s is the width of the slot cut, L_e the effective length of the MSA, and c the phase velocity of the wave. The problem found in the miniaturized slotted MSA for a TM_{01} mode of operation is the increased X-pol effect [11, 12]. The fringing field distribution along the periphery of the MHMSA is as shown in Fig. 1(c).

3. DESIGN OF CSRR-MHMSA

From Fig. 1(c), it is observed that undesired fringing electric field E_x is oriented along x-axis causing an increased X-pol effect. This problem is minimized by increasing the polarizability of the fringing electric field at both radiating edges along y-axis. As shown in Fig. 2(a), the polarizability of electric and magnetic fields is increased by using CSRR arrays placed at the ground below radiating edges of the patch.

3.1. Design of CSRR

Fig. 2(a) shows the structure of CSRR. As discussed above, the CSRR increases both electric and magnetic polarizabilities at the resonance frequency. The resonance frequency of the CSRR is given by Eq. (2) [13],

$$f_0 = \frac{2}{2\pi l C_{pul} L} \tag{2}$$

where l is the average length (perimeter) of the resonator, C_{pul} per unit length capacitance, and L is the inductance of the resonator. CSRR is available in circular and rectangular shapes, but to obtain the polarization of the electric field in y-direction, rectangular CSRR is selected. CSRRs are located on ground plane at distance $d = 0.64\,\text{mm}$ from the radiating edges of patch. CSRRs are excited by fringing electric field, where $d \leq \Delta L = h/\sqrt{\varepsilon_r}$. Perimeter of the CSRR is less than $\lambda/2$. Under this assumption, the current at region B (gap) is maximum, whereas the current is minimum at region A (opposite to the gap). So the electric field is maximum at region B and directed along y axis. In region C of CSRR, lines
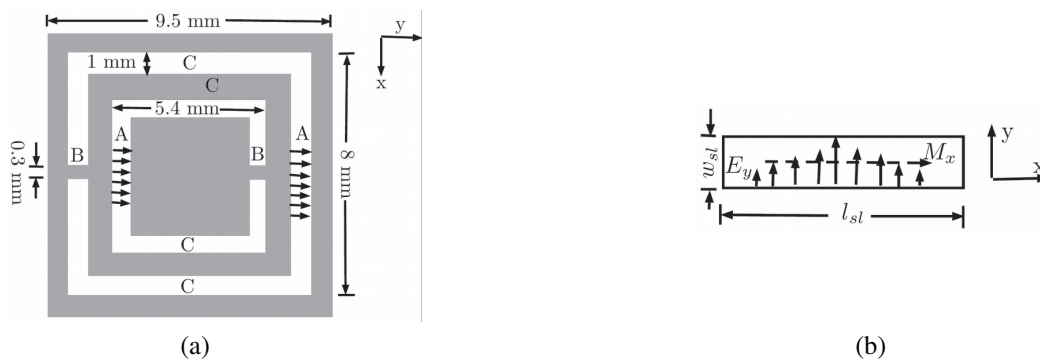

(a)

(b)

Figure 2. Complementary split ring resonator (CSRR) and single slot. (a) Electrical field distribution on CSRR. (b) Single slot of S-CSRR-MHMSA.

of the electric field are opposite to each other and hence cancel. For single edge segment of rectangular CSRR, the polarizability in y-direction is given by Eq. (3),

$$p_y = \alpha_{yy}^{ee} E_y^0 + \alpha_{yz}^{em} B_z^0 \tag{3}$$

where p_y is the electric dipole along y axis, E_y^0 the electric field along y axis, and α_{yy}^{ee} the polarizability constant which depends on y directed electric field. Also, CSRR exhibits some non-resonant electric polarizability in y and z directions. The electric dipole generated at non-resonant frequencies due to magnetic field B_z^0 and polarizability α_{yz}^{em} are neglected at the resonance frequency.

4. DESIGN OF SLOTS AND CSRR LOADED MHMSA (S-CSRR-MHMSA)

Due to the conductor dielectric boundary condition, electric fields at non-radiating edges of the MHMSA are oriented along x-direction as shown in Fig. 1(c). This increases the cross-polarization effect of the miniaturized antenna. The undesired electric field in the x-direction is suppressed by cutting an array of slots at both non-radiating edges, as shown in Fig. 3(b). This slot array is perpendicular to the non-radiating edges. As shown in Fig. 2(b), the length of each slot in the array is in between $\lambda/10 < l_{sl} < \lambda/2$, and width w_{sl} is less than $\lambda/10$ so that maximum electric field in y-direction is obtained at center of the slot. Slots in an array are excited by the fringing field. This develops magnetic surface current $\bar{M}$ in slots along the x-axis and is given by Eq. (4).

$$\bar{M} = E_y \bar{a}_y \times \bar{a}_z = E_y \bar{a}_x \tag{4}$$

The slot length $l_{sl} = 6\,\text{mm}$ and slot width $w_{sl} = 1\,\text{mm}$ are selected for this design, where electric field $E_y = E_0 \cos(\pi x/l_{sl})$. The slot array placed in the ground also helps to increase the inductance by increasing the length of the current path. So, the inductance of the parallel RLC resonant antenna circuit model is increased, and the resonant frequency of the circuit model is decreased. Thus, the microstrip antenna is further miniaturized [12, 14, 15].
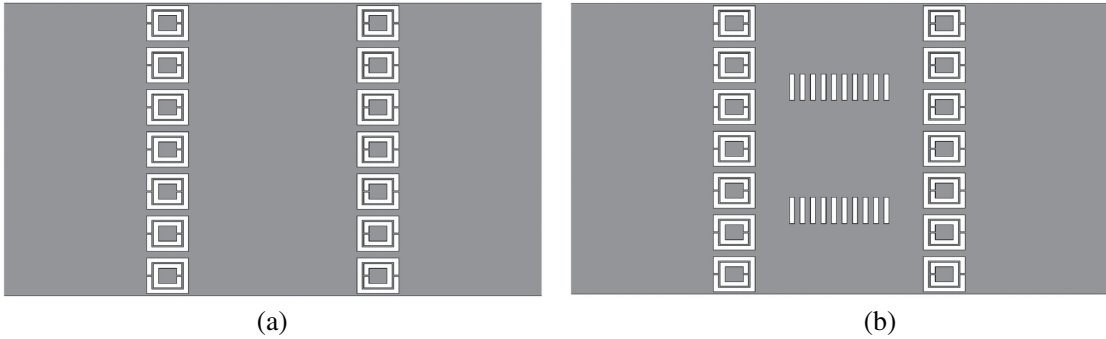

(a)   (b)

Figure 3. Antenna bottom view. (a) CSRR-MHMSA. (b) S-CSRR-MHMSA.

5. RESULTS AND DISCUSSIONS

In this section, results of MSA and MHMSA are compared. Further MHMSA is compared with CSRR-MHMSA and S-CSRR-MHMSA. All antennas are simulated using ANSYS HFSS. These antennas are fabricated and tested using VNA ZVL13 make R & S® in Antenna and Wave Propagation lab, Rajarambapu Institute of Technology, Sakharale, Sangli, Maharashtra, India. Fig. 4 shows the photographs of fabricated antennas. The radiation pattern measurement has been carried out in open space by ensuring that there is no reflection from other objects. A photograph depicting experimental setup for $|S_{11}|$ measurement and VSWR measurement is shown in Fig. 5.
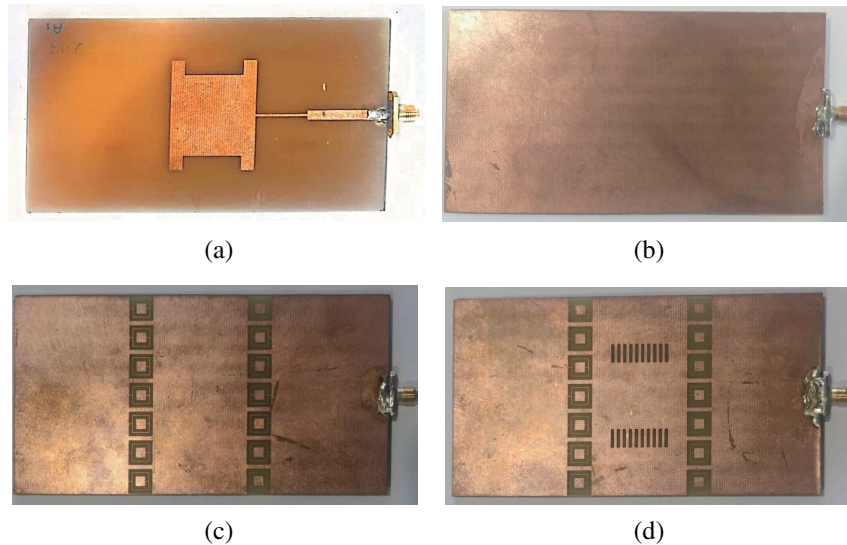
(a)   (b)

(c)   (d)

Figure 4. Fabricated antennas. (a) MHMSA, CSRR-MHMSA, S-CSRR-MHMSA top view. (b) MHMSA bottom view. (c) CSRR-MHMSA bottom view. (d) S-CSRR-MHMSA bottom view.

Figure 5. Experimental setup. Setup for $|S_{11}|$ plot, VSWR and Z measurement.

5.1. Comparison of MSA and MHMSA

Simulated frequency versus $|S_{11}|$ graph is shown in Fig. 6. The MSA is operating at 2.375 GHz, whereas MHMSA is operating at 2.13 GHz. Comparison of MSA and MHMSA with respect to simulated antenna parameters such as resonant frequency f_r, antenna length L, percentage miniaturization (% Mini.), reflection coefficient $|S_{11}|$, voltage standing wave ratio VSWR and X-pol are shown in Table 1. The frequency of MHMSA is shifted to left. Thus, the size of the MHMSA is reduced by 12%. From Fig. 7(a) it is clear that though the size of MHMSA is reduced, the X-pol level of the MHMSA is increased as compared to the X-pol level of MSA. The X-pol of MHMSA and MSA at direction of maximum radiation $(\phi = 0^0)$ is -39.96 dB and -49.72 dB, respectively. The X-pol level of the miniaturized MHMSA is increased by 9.76 dB, which is significantly large.
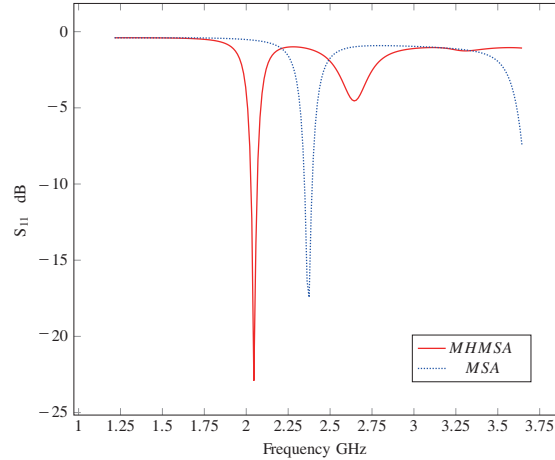
Figure 6. Simulated and Measured $|S_{11}|$ plots.

Table 1. Antenna comparison with respect to simulated-resonance frequency f_r, antenna length L, reflection coefficient S_{11}, percentage miniaturization% Mini., VSWR and X-pol.

Antenna	f_r [GHz]	L	% Mini	S_{11} [dB]	VSWR	X-Pol [dB]
MSA	2.375	$\lambda/2$	0	-17.438	1.35	-49.72
MHMSA	2.13	$\lambda/2.29$	12	-26.40	1.10	-39.96
CSRR-MHMSA	2.13	$\lambda/2.29$	12	-29.28	1.07	-55.40
S-CSRR-MHMSA	2.04	$\lambda/2.32$	15	-22.9130	1.15	-44.97

Table 2. Antenna comparison with respect to simulated and measured directivity D, gain G, and %η.

Antenna	D[dB]		G[dB]		%η	
	Sim.	Meas.	Sim.	Meas.	Sim.	Meas.
MHMSA	4.44	4.44	3.99	3.40	89.83	78.70
CSRR-MHMSA	4.46	4.63	4.06	3.70	91.03	80.72
S-CSRR-MHMSA	4.33	4.40	3.96	4.00	91.46	91.20

5.2. Comparison of MHMSA, CSRR-MHMSA, S-CSRR-MHMSA

The X-pol levels of MHMSA, CSRR-MHMSA, and S-CSRR-MHMSA are compared in Fig. 7(b). The X-pol level of the CSRR-MHMSA is -55.40 dB. The X-pol level of the S-CSRR-MHMSA is comparatively greater than that of the CSRR-MHMSA, because S-CSRR-MHMSA is miniaturized by 15%. The antenna comparison with respect to percentage miniaturization is illustrated in Table 1. The X-pol level of the S-CSRR-MHMSA is -44.97 dB, which is still less than that of the MHMSA. Simulated and measured directivities D, gains G, and percentage radiation efficiencies %η are compared in Table 2. It is observed that X-Pol is decreased without degradation of directivity D, radiation efficiency η, and gain G of CSRR-MHMSA and S-CSRR-MHMSA. Fig. 8 shows simulated and measured frequencies versus $|S_{11}|$ for MHMSA, CSRR-MHMSA, and S-CSRR-MHMSA, whereas Fig. 9 shows simulated and measured frequencies versus VSWR for MHMSA, CSRR-MHMSA, and S-CSRR-MHMSA. A good agreement between simulated and measured results is observed. Simulated and Measured BWs, $|S_{11}|$, and VSWRs of these antennas are shown in Table 3. Low VSWR and $|S_{11}|$ at operating frequency indicate that
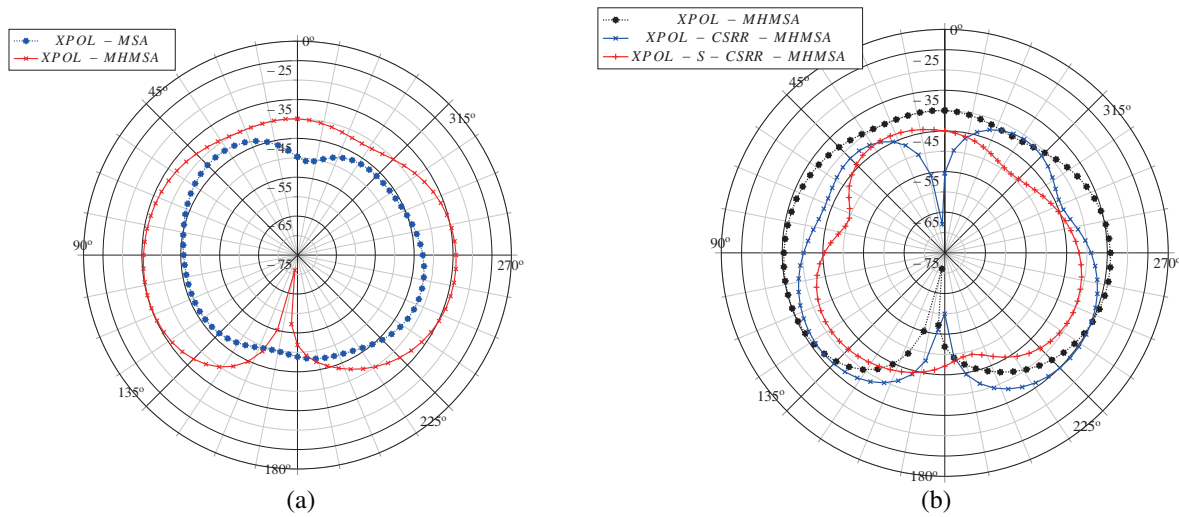
Figure 7. Simulated E plane X-pol [dB]. (a) MSA and MHMSA. (b) MHMSA, CSRR-MHMSA and S-CSRR-MHMSA.

these modified antennas do not have the problem of impedance mismatch, even though the ground is defected by cutting slots and CSRR placement. In Table 4, the CP-XP isolations in E-plane and H-plane of proposed antennas are compared. The CP-XP isolation in dB is calculated by subtracting X-pol level [dB] from Co-pol level [dB] at an angle of maximum radiations ($\phi = 0°$). Simulated and measured CP-XP isolations of the CSRR-MHMSA and S-CSRR-MHMSA are greater than that of the MHMSA. The CP-XP isolation for CSRR-MHMSA and S-CSRR-MHMSA is above the acceptable level of 20 dB. The array of slots and CSRR at the ground increase the polarizability of the electric field E_y in y-direction, and therefore CP-XP isolation level is increased.

Table 3. Simulated and Measured f_r, BW, S_{11}, and VSWR of MHMSA, CSRR-MHMSA and S-CSRR-MHMSA.

Antenna	f_r [GHz]		BW [MHz]		S_{11} [dB]		VSWR	
	Sim.	Meas.	Sim.	Meas.	Sim.	Meas.	Sim.	Meas.
MHMSA	2.13	2.13	40.4	40	−26.40	−20.23	1.10	1.18
CSRR–MHMSA	2.13	2.13	42.5	35	−29.28	−14.37	1.07	1.147
S-CSRR–MHMSA	2.04	2.04	39	40	−22.91	−20.36	1.15	1.126

Table 4. Simulated and measured Z_{in} and CP-XP isolation of MHMSA, CSRR-MHMSA and S-CSRR-MHMSA.

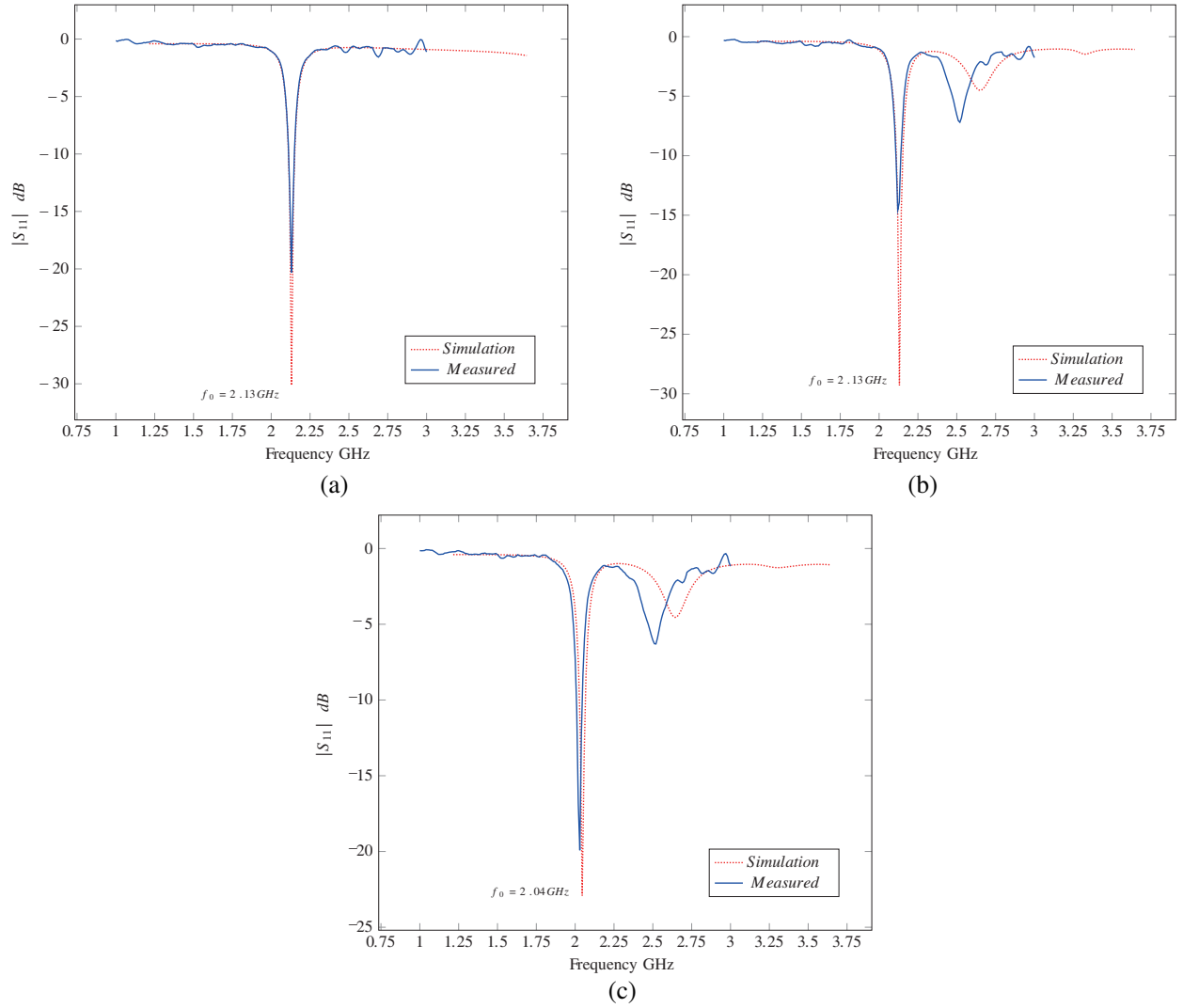| Antenna	Z_{in} [Ω]		CP-XP isolation [dB]			
			E-Plane		H-Plane	
	Sim.	Meas.	Sim.	Meas.	Sim.	Meas.
MHMSA	51.85+j4.51	57.86+j4.038	39.96	21.7	44.96	23
CSRR–MHMSA	52.47+j2.5	71.97+j7.98	55.40	29	55.40	27
S-CSRR–MHMSA	52.11+j7.01	52.93+ j8.99	44.97	26.73	45.97	24.5

(a)

(b)

(c)

Figure 8. Simulated and measured $|S_{11}|$ plots. (a) MHMSA $|S_{11}|$ plot. (b) CSRR-MHMSA $|S_{11}|$ plot. (c) S-CSRR-MHMSA $|S_{11}|$ plot.

5.2.1. Normalized Radiation Pattern

The two antenna method is used to draw the normalized radiation patterns of the proposed antennas. The half wavelength dipole antenna of gain 2.1 dB as a reference antenna is connected at the generator port (port 1), while the antenna under test (AUT) is connected to port 2 of the VNA. At the desired frequency, the forward transmission coefficient S_{21} dBm is measured in the E plane by rotating AUT about z-axis from $\phi = 0°$ to $360°$ with step angle $5°$. Both E plane Co-polarization (Co-pol) and Cross-polarization (X-pol) levels are measured. The setup for the E plane Co-pol and X-pol pattern measurement is shown in Fig. 10. The measured S_{21} is normalized and compared with the simulated normalized E plane field pattern. The polar plots of the normalized radiation E-plane and H-plane field patterns in dB scale are shown in Fig. 11 and Fig. 12, respectively. The radiation patterns for CSRR-MHMSA and S-CSRR-MHMSA are stable, which means that the shapes of radiation patterns of these antennas are same as that of the MHMSA. Simulated and Measured normalized levels of CP-XP isolation for MHMSA, CSRR-MHMSA, and S-CSRR-MHMSA are given in Table 4.
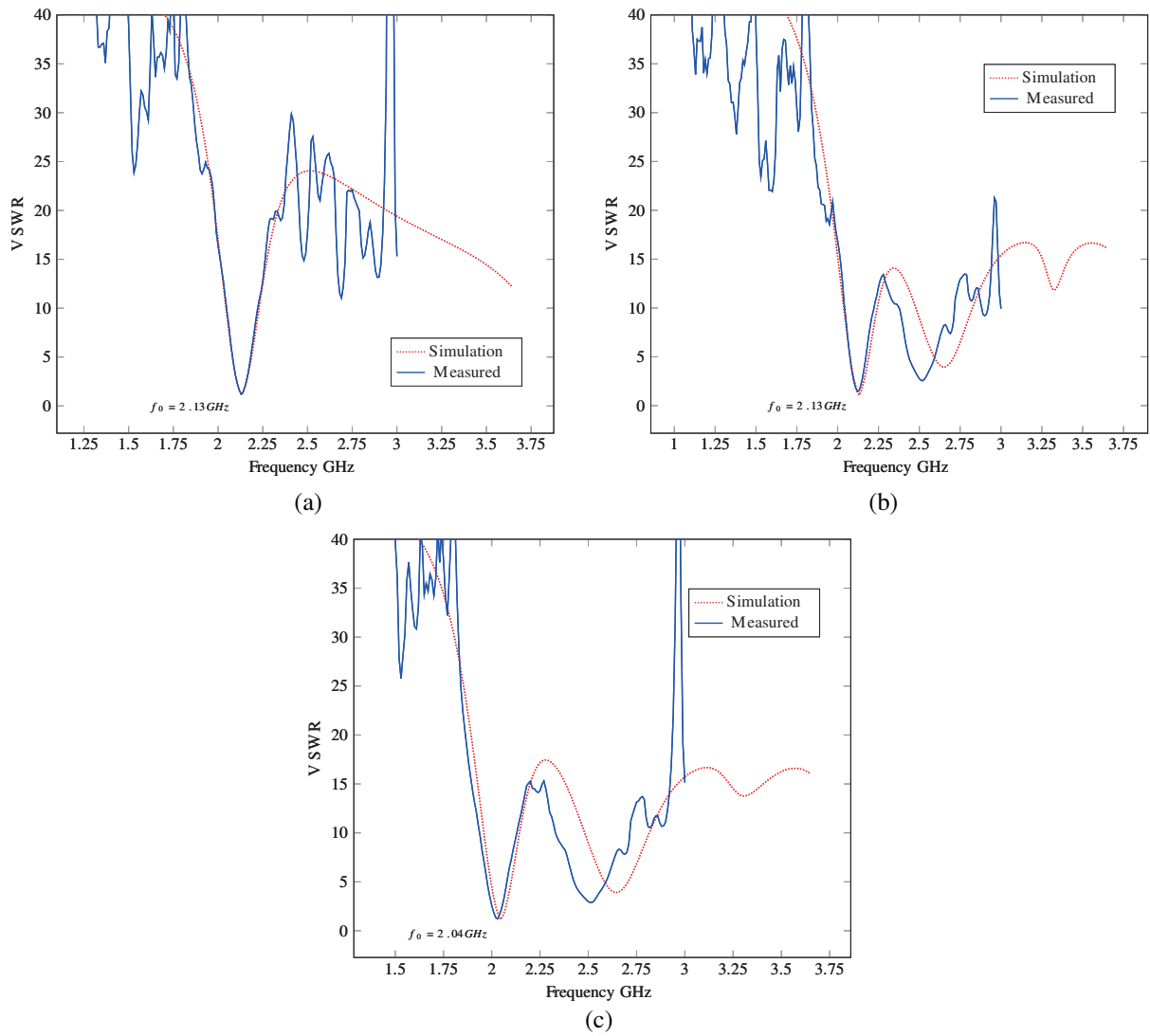
Figure 9. Simulated and measured VSWR plots. (a) MHMSA VSWR plot. (b) CSRR-MHMSA VSWR plot. (c) S-CSRR-MHMSA VSWR plot.
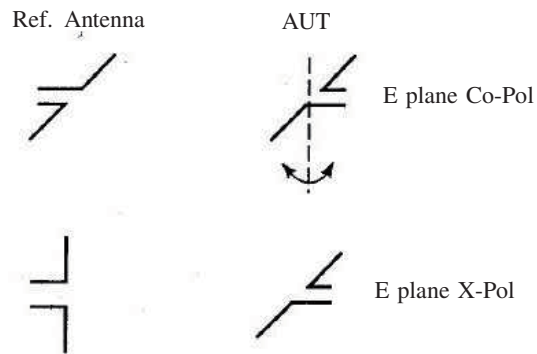

Figure 10. Setup prototype for measurement of E plane Co-pol and X-pol.
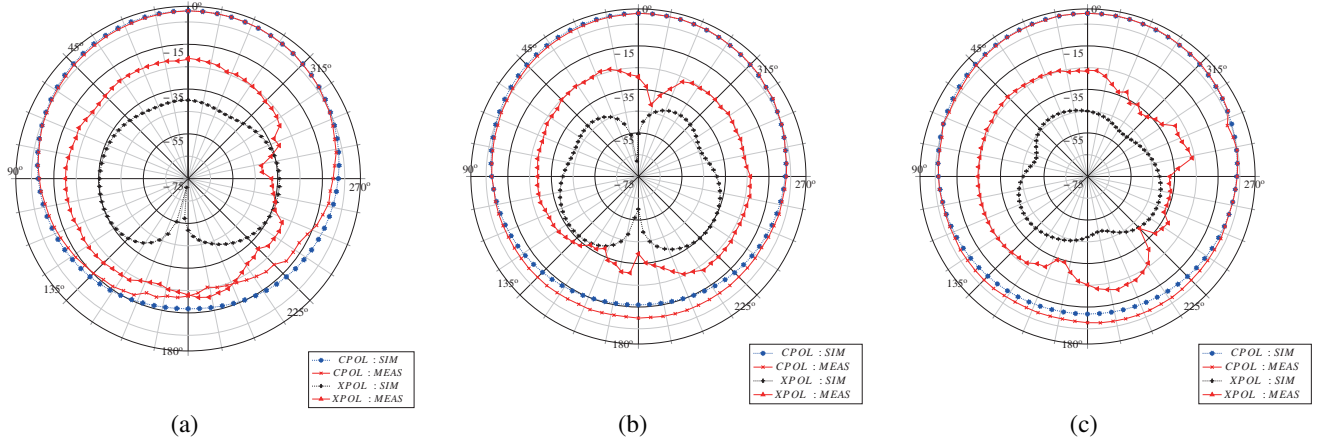
Figure 11. Simulated and measured normalized E plane radiation field pattern [dB]. (a) MHMSA, $f_r = 2.13$ GHz. (b) CSRR-MHMSA, $f_r = 2.13$ GHz. (c) S-CSRR-MHMSA, $f_r = 2.04$ GHz.

Figure 12. Simulated and measured normalized H plane radiation field pattern [dB]. (a) MHMSA, $f_r = 2.13$ GHz. (b) CSRR-MHMSA, $f_r = 2.13$ GHz. (c) S-CSRR-MHMSA, $f_r = 2.04$ GHz.
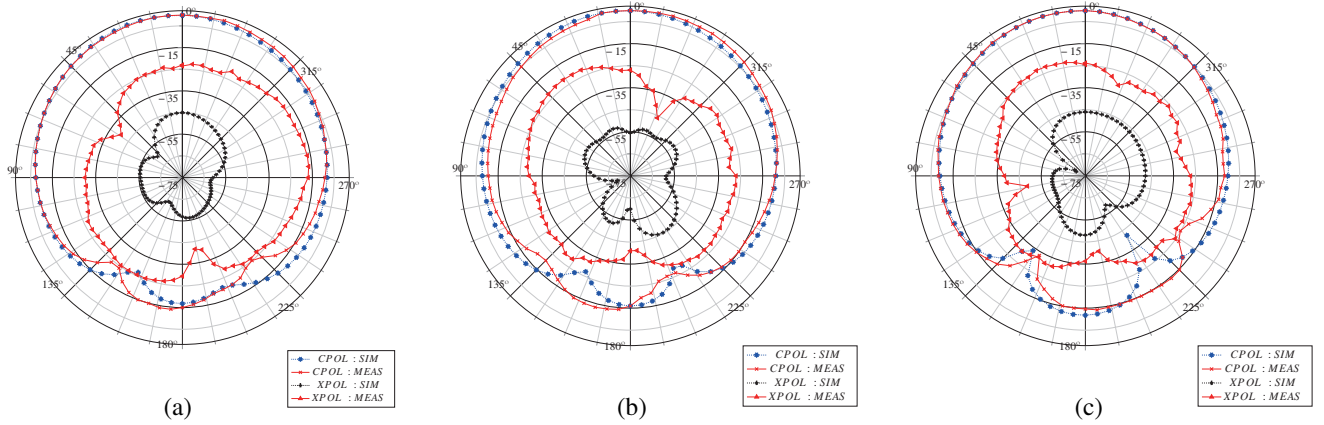
6. CONCLUSION

From observations, it has been concluded that the X-pol level of the miniature MHMSA is increased by 9.76 dB compared to the conventional MSA. To reduce the X-pol level, conductor-dielectric boundary condition (electric field is always normal to the conductor boundary) is used. Therefore, CSRRs and slots are designed and positioned in such a way that the lines of the electric field are oriented in desired direction (y-direction) due to increased polarizability. Compared to MHMSA, the measured X-pol levels of CSRR-MHMSA and S-CSRR-MHMSA are decreased by 7.3 dB and 5.04 dB, respectively. Miniature MHMSA, CSRR-MHMSA, and miniaturized S-CSRR-MHMSA have been designed, fabricated, and tested. A comparative study of these antennas has been carried out with respect to measured and simulated $|S_{11}|$, BWs, VSWRs, impedances, and normalized radiation patterns. The measured CP-XP isolation levels of the CSRR-MHMSA and S-CSRR-MHMSA in E-plane are 29 dB and 26.73 dB, respectively, and in H-plane are 27 dB and 24.5 dB, respectively, which are above the acceptable level of 20 dB. Good agreement between measured and simulated results has been observed.

REFERENCES

1. Ludwig, A., "The definition of cross polarization," *IEEE Transactions on Antennas and Propagation*, Vol. 21, No. 1, 116–119, 1973.

2. Hansen, R., "Cross polarization of microstrip patch antennas," *IEEE Transactions on Antennas and Propagation*, Vol. 35, No. 6, 731–732, 1987.

3. Balanis, C. A., *Antenna Theory: Analysis and Design*, John wiley & sons, 2015.

4. Tienda, C., M. Younis, and G. Krieger, "Reduction of cross-polarization on a single offset parabolic reflector using digital beam forming techniques and combination of elements," *Proceedings of EUSAR 2016: 11th European Conference on Synthetic Aperture Radar*, 1–3, VDE, 2016.

5. Chopra, R., G. Kumar, and R. Lakhmani, "Corner fed microstrip antenna array with reduced cross polarization and side lobe level," *2016 Asia-Pacific Microwave Conference (APMC)*, 1–4, IEEE, 2016.

6. Chin, C., Q. Xue, H. Wong, and X. Zhang, "Broadband patch antenna with low cross-polarisation," *Electronics Letters*, Vol. 43, No. 3, 137–138, 2007.

7. Chen, X., D. Wu, L. Yang, and G. Fu, "Compact circularly polarized microstrip antenna with cross-polarization suppression at low-elevation angle," *IEEE Antennas and Wireless Propagation Letters*, Vol. 16, 258–261, 2016.

8. Kumar, J., B. Basu, F. A. Talukdar, and A. Nandi, "Multimode-inspired low cross-polarization multiband antenna fabricated using graphene-based conductive ink," *IEEE Antennas and Wireless Propagation Letters*, Vol. 17, No. 10, 1861–1865, 2018.

9. Ghosh, C. K. and S. K. Parui, "Cross-polarization reduction of e-shaped microstrip array using spiral-ring resonator," *Progress In Electromagnetics Research*, Vol. 38, 217–227, 2013.

10. Manikandan, R. and P. K. Jawahar, "Cross polarization reduction of circularly polarized microstrip antenna with SRR," *International Journal of Control Theory and Applications, International Science Press*, Vol. 10, No. 9, 613–618, 2017.

11. Kumar, G. and K. P. Ray, *Broadband Microstrip Antennas*, Artech house, 2003.

12. Mulla, S. S. and S. S. Deshpande, "Miniaturization of multiband annular slot ring antenna using reactive loading," *Journal of Electromagnetic Waves and Applications*, Vol. 32, No. 14, 1779–1790, 2018.

13. Marqués, R., F. Martin, and M. Sorolla, *Metamaterials with Negative Parameters: Theory, Design, and Microwave Applications*, Vol. 183, John Wiley & Sons, 2011.

14. Garg, R., P. Bhartia, I. J. Bahl, and A. Ittipiboon, *Microstrip Antenna Design Handbook*, Artech House, 2001.

15. Kumar, J., B. Basu, and F. Talukdar, "Modeling of a PIN diode RF switch for reconfigurable antenna application," *Scientia Iranica*, Vol. 26, No. 3, 1714–1723, 2019.